

A UV ULTRA-LUMINOUS LYMAN BREAK GALAXY AT $Z = 2.78$ IN NDWFS BOÖTES FIELD^{1,2,3}

FUYAN BIAN, XIAOHUI FAN, LINHUA JIANG

Steward Observatory, University of Arizona, 933 N. Cherry Ave. Tucson, AZ, 85721, USA

ARJUN DEY

National Optical Astronomy Observatory, 950 North Cherry Avenue, Tucson, AZ 85719, USA

RICHARD F. GREEN

Large Binocular Telescope Observatory, University of Arizona, 933 N. Cherry Ave., Tucson, AZ 85721, USA

ROBERTO MAIOLINO

INAF Osservatorio Astronomico di Roma Via di Frascati 33 IT 00040 Monte Porzio Catone Italy and
Cavendish Laboratory, Univerisy of Cambridge, 19 J. J. Thomson Ave., Cambridge CB3 0HE, UK

FABIAN WALTER

Max-Planck-Institut für Astronomie, Königstuhl 17, D-69117 Heidelberg, Germany

IAN MCGREER, RAN WANG

Steward Observatory, University of Arizona, 933 N. Cherry Ave. Tucson, AZ, 85721, USA

YEN-TING LIN

Institute of Astronomy and Astrophysics, Academia Sinica, Taipei, Taiwan ; Institute for the Physics and Mathematics of the Universe,
Todai Institutes for Advanced Study, The University of Tokyo, Kashiwa, Chiba, Japan

ABSTRACT

We present one of the most ultraviolet (UV) luminous Lyman Break Galaxies (LBGs) (J1432+3358) at $z = 2.78$, discovered in the NOAO Deep Wide-Field Survey (NDWFS) Boötes field. The R -band magnitude of J1432+3358 is 22.29 AB, more than two magnitudes brighter than typical L^* LBGs at this redshift. The deep z -band image reveals two components of J1432+3358 separated by $1.''0$ with flux ratio of 3:1. The high signal-to-noise ratio (S/N) rest-frame UV spectrum shows $\text{Ly}\alpha$ emission line and interstellar medium absorption lines. The absence of N V and C IV emission lines, the non-detection in X-ray and radio wavelengths and mid-infrared (MIR) colors indicate no or weak active galactic nuclei (AGN) ($< 10\%$) in this galaxy. The galaxy shows broader line profile with the full width half maximum (FWHM) of about 1000 km s^{-1} and larger outflow velocity ($\approx 500 \text{ km s}^{-1}$) than those of typical $z \sim 3$ LBGs. The physical properties are derived by fitting the spectral energy distribution (SED) with stellar synthesis models. The dust extinction, $E(B - V) = 0.12$, is similar to that in normal LBGs. The star formation rates (SFRs) derived from the SED fitting and the dust-corrected UV flux are consistent with each other, $\sim 300 \text{ M}_\odot \text{ yr}^{-1}$, and the stellar mass is $(1.3 \pm 0.3) \times 10^{11} \text{ M}_\odot$. The SFR and stellar mass in J1432+3358 are about an order of magnitude higher than those in normal LBGs. The SED-fitting results support that J1432+3358 has a continuous star formation history with the star formation episode of $6.3 \times 10^8 \text{ yr}$. The morphology of J1432+3358 and its physical properties suggest that J1432+3358 is in an early phase of 3:1 merger process. The unique properties and the low space number density ($\sim 10^{-7} \text{ Mpc}^{-3}$) are consistent with the interpretation that such galaxies are either found in a short unobscured phase of the star formation or that small fraction of intensive star-forming galaxies are unobscured.

Subject headings: galaxies: high-redshift — galaxies: individual (J1432+3358) — galaxies: star formation

¹ Based on observations obtained at the Gemini Observatory, which is operated by the Association of Universities for Research in Astronomy, Inc., under a cooperative agreement with the NSF on behalf of the Gemini partnership: the National Science Foundation (United States), the Science and Technology Facilities Council (United Kingdom), the National Research Council (Canada), CONICYT (Chile), the Australian Research Council (Australia), Ministério da Ciência, Tecnologia e Inovação (Brazil) and Ministerio de Ciencia, Tecnología e Innovación Pro-

ductiva (Argentina)

² Based on data acquired using the Large Binocular Telescope (LBT). The LBT is an international collaboration among institutions in the United States, Italy and Germany. LBT Corporation partners are: The University of Arizona on behalf of the Arizona university system; Istituto Nazionale di Astrofisica, Italy; LBT Beteiligungsgesellschaft, Germany, representing the Max-Planck Society, the Astrophysical Institute Potsdam, and

Heidelberg University; The Ohio State University, and The Research Corporation, on behalf of The University of Notre Dame, University of Minnesota and University of Virginia.

³Based on [in part] data collected at Subaru Telescope, which is operated by the National Astronomical Observatory of Japan.

1. INTRODUCTION

Over the last decade, the dropout method (the Lyman break technique), which uses the fact that little flux is emitted bluewards of the Lyman limit (912 Å), has been fundamental in searching for high-redshift star-forming galaxies (e.g., Steidel et al. 1996). Spectroscopic follow-up observations show that the efficiency of this method is high (e.g., Steidel et al. 2003, 2004). Large samples of Lyman Break Galaxies (LBGs) from $z \sim 2$ up to $z \sim 10$ have been established (e.g., Bouwens et al. 2008, 2011). These samples of LBGs provide crucial information on determining the cosmic star formation history (e.g., Madau et al. 1996; Lilly et al. 1996; Cowie et al. 1996), mapping the growth of large scale structures (e.g., Adelberger et al. 1998; Giavalisco et al. 1998; Lee et al. 2006, 2009), and studying the properties of dark matter halos hosting the LBGs.

Optical and near-infrared (NIR) photometric and spectroscopic observations of these galaxies reveal the properties of the UV-selected galaxies at $z \sim 2-3$. The median stellar mass of the $z \sim 3$ LBGs is about $2.4 \times 10^{10} M_{\odot}$ (e.g., Shapley et al. 2001), and the mean star formation rate (SFR) derived from the H α and UV luminosity is about $30 M_{\odot} \text{ yr}^{-1}$ (e.g., Erb et al. 2006b). The median dust extinction ($E(B - V)$) is around 0.15 (e.g., Shapley et al. 2001). The $z \sim 2-3$ LBGs show compact morphologies (half-light radii, $r_e < 0''.5$) in Hubble space telescope (HST) images (e.g., Giavalisco 1998).

However, most of optical/NIR surveys for high-redshift galaxies are deep field surveys with survey area less than 1 deg^2 . So far, the largest $z \sim 2-3$ LBGs survey with spectroscopic redshifts only covers a total area of around one deg^2 with > 2000 spectroscopic redshifts (e.g., Steidel et al. 2003; Reddy & Steidel 2009). Due to the small survey volume, combined with the rapid decline of galaxy luminosity function at the bright end, these surveys are not suited to reveal the most luminous and most massive systems; previous studies have been focusing on the LBGs with luminosity of L^* or sub- L^* ($r > 24.5$). A sample of bright LBGs was discovered in Sloan Digital Sky Survey (SDSS), however, HST follow-up observations show that these galaxies are unresolved point sources indicating that these objects are quasars rather than galaxies (Bentz et al. 2008). To date only one unlensed LBG at $z \sim 3$ with R -band magnitude brighter than 22.5 has been found (Cooke et al. 2008). The nature and properties of this type of galaxy are still unknown, so it is important to build up a sample of these UV ultra-luminous galaxies and perform detailed follow-up observations on them.

Finding UV ultra-luminous $z \sim 2-3$ galaxies requires wide-field surveys with deep, multi-color broad band images. In this paper, we report a UV ultra-luminous LBG, J1432+3358, with $R_{AB} = 22.29$ at $z = 2.78$ discovered in the NOAO Deep Wide Field Survey (NDWFS) Boötes field. Through this paper, we adopt $\Omega_m = 0.3$, $\Omega_{\Lambda} = 0.7$, and $H = 70 \text{ km s}^{-1} \text{ Mpc}^{-1}$ (Spergel et al. 2007). All the magnitudes are AB magnitudes.

2. OBSERVATIONS

In 2008 and 2009, we carried out deep U - and Y -band imaging of the 9 deg^2 NOAO Deep Wide-Field Survey (NDWFS) Boötes Field (Jannuzi & Dey 1999). Our sur-

vey used the $2 \times 8.4 \text{ m}$ Large Binocular Telescope (LBT) (Hill et al. 2010) equipped with two prime focus Large Binocular Cameras (LBC, Giallongo et al. 2008). This new LBT survey builds on the available unique multi-wavelength data of the NDWFS Boötes field and fills in two critical wavelength gaps at 3500 Å and $1 \mu\text{m}$ with the U and Y bands. The deep U -band images (25.2 AB magnitude with 5σ detection), together with the existing B_W - and R -band images taken with the Mosaic CCD camera on Kitt Peak 4 m Mayall telescope, allow us to search for the star-forming galaxies at $z \sim 3$ using the U -dropout technique, and total 15,000 LBG candidates are selected based on the $U - B_W$ and $B_W - R$ color-color diagram, with the selection criterion being

$$\begin{aligned} U - B_W &> 1.0, \\ B_W - R &< 1.9, \\ B_W - R &< U - B_W - 0.1, \\ R &< 25.0. \end{aligned} \quad (1)$$

The typical image quality in the R -band is $1''$ and thus can not resolve typical LBGs. Nevertheless, the large survey area allows us to select and study the most UV luminous LBGs at $z \sim 3$ with $R < 22.5$ ($L > 7L^*$ at $z \sim 3$).

Spectroscopic follow-up observations of 12 of bright LBG candidates were obtained using the blue channel spectrograph on 6.5 m Multiple Mirror Telescope (MMT) on 2010 April 15. Typically 20-40 minutes exposures were taken for each candidate. The wavelength coverage is $4000-7500 \text{ Å}$. One out of 12 candidates was confirmed as a UV ultra-luminous LBG (J1432+3358) at $z = 2.78$, and the coordinates of this galaxy are R.A.= $14^{\text{h}}32^{\text{m}}21^{\text{s}}.84$ and Decl.= $33^{\circ}58'18''.2$, J2000. The remaining eleven candidates are all quasars in the redshift range of $2 < z < 3$. All these quasars show broad Ly α , N V, and C IV emission lines and they are all point sources.

A high signal-to-noise ratio (S/N) spectrum of J1432+3358 was obtained with the 8.2 m Gemini-N telescope and GMOS instrument on 2011 March 9 and 10 (Program ID: GN-2011-C-5). The sky was clear and the resulting image quality was $0''.6 - 0''.7$. The total exposure time was 4 hr and was divided into eight 30-min individual exposures. The slit width was $1''$. The B600-G5307 grating was used, and two central wavelengths of 5200 Å and 5300 Å were used to fill the gaps between different CCD chips. The wavelength coverage was from 4000 Å to 6500 Å , and the spectral resolution ($R = \lambda/\delta\lambda$) is 850. The airmass of the object during the observing was about 1.05, thus we did not use the parallactic angle. The slit oriented in P.A.= -60 degrees (300 degrees), which was roughly along the galaxy extended direction (Figure 1). The spectrophotometric standard G191-B2B was observed for flux calibration, and a CuAr arc lamp was used for wavelength calibration. The spectra were reduced and calibrated using standard Gemini IRAF package. The final spectrum has been smoothed by 4 Å . The S/N per spectral element ($\sim 4 \text{ Å}$) is 8-10.

MIR photometry of J1432+3358 was obtained by the Spitzer Deep Wide-Field Survey (Ashby et al. 2009). In addition, H -band image with one hour exposure was obtained using the SWIRC on 6.5 m MMT on 2012 Janu-

rary 5. We also got deep z -band image from the Subaru B ϕ otes field survey (B ϕ otesZ Survey) (Y. Lin et al. 2012, in preparation). The image quality of the z -band image is $0''.5$. The total magnitudes of J1432+3358 are measured with SExtractor (Bertin & Arnouts 1996), and are listed in table 1.

3. RESULTS

3.1. Lensed or Unlensed?

In the last decade, a sample of bright lensed high-redshift galaxies has been established through systematic searches towards galaxy clusters (e.g. Mehlert et al. 2001; Sand et al. 2005) and red galaxies in the SDSS images (e.g. Smail et al. 2007; Allam et al. 2007; Diehl et al. 2009; Lin et al. 2009). It is crucial to determine whether J1432+3358 is lensed or not. Studies suggest that the total fraction of high-redshift galaxies and quasars that are lensed is small (e.g., Turner et al. 1984; Jain & Lima 2011), but the lensing contribution becomes larger with increasing brightness. Jain & Lima (2011) find that the lensing contribution becomes significant when $L > 10L^*$, and about 1/3-1/2 of the LBGs with $L = 7L^*$ are lensed galaxies (van der Burg et al. 2010).

The structure of J1432+3358 is well resolved by the ground-based imaging observations. The broad band U -, B_W -, R -, I -, z - and Y -band images (Figure 1) of J1432+3358 show extended morphology. The deep multi-band images show that there is no foreground lensing galaxy and the morphology of the galaxy is also consistent with being unlensed. Especially, in the deep Subaru z -band image with image quality of $0''.5$, J1432+3358 is resolved into two components, and separation of these two parts is by $1''.0$ (7.8 kpc). These two components do not show stretched arc structures at the resolution of the image. Furthermore, the central wavelengths of Ly α emission from these two components have a small offset (237 ± 23 km s $^{-1}$) and the Ly α flux ratio of these two components is not consistent with the continuum flux ratio of these two components (see detail in section 3.3). Meanwhile, the spectrum of J1432+3358 does not show any other redshift systems that could be from the lensing galaxy. Therefore, we conclude that J1432+3358 is not a lensed galaxy.

3.2. Morphology

The deep z -band image reveals two components in J1432+3358. We use GALFIT (Peng et al. 2002) to fit the light distribution of these two components with either exponential disk or DeVaucouleurs profiles. We find that the DeVaucouleurs profile is better to fit the brighter component and the exponential disk is better to fit the fainter component. The effective radius are $0''.26 \pm 0''.03$ and $0''.21 \pm 0''.03$, respectively, which correspond to about 2.0 kpc in physical size. This size is comparable to the typical size of LBGs at $z \sim 3$ (e.g. Ferguson et al. 2004). The distance between these two components is about $1''.0$, which is about 7.8 kpc. The brightness ratio between these two components in J1432+3358 is 3 to 1. Assuming a simple relation between luminosity and stellar mass, the mass ratio of the two components is also 3 to 1 implying that it is a 3:1 merger. These two components are barely resolved by the z -band image. Further

high resolution HST follow-up imaging observations will help us to fit the systems more accurately and to reveal more detailed structure of this galaxy.

The morphology of J1432+3358 in B_W -band image and that in R - and I -band images look different (figure 1). To characterize the morphology in these bands, we use GALFIT to model the galaxy light distribution in the B_W -, R -, and I -band images of J1432+3358. The Sérsic profile (Sérsic 1963) is used to fit the light profile of J1432+3358. The GALFIT fitting results are listed in table 1. The R - and I -band morphologies of J1432+3358 can be well fit by a disk-like profile with Sérsic index $n \approx 1.3$, while the Sérsic index is about 3.10 for the morphology in B_W -band image, which is much larger than that in R - and I -band images (Table 1). Furthermore, the galaxy light distribution in B_W -band image can not be well fitted by a single Sérsic profile component, with reduced chi-square of 1.310. The B_W -band morphology is round rather than elongated. The strong Ly α emission line lies within the B_W filter at the redshift of 2.78. We therefore interpret the diffuse B_W morphology as being likely due to a diffuse Ly α halo around J1432+3358 (c.f., Steidel et al. 2011). The Ly α photons from the central galaxy are scattered by the neutral hydrogen gas in the galaxy's circum-galactic medium (CGM) and form the diffuse Ly α halo. We do not carry out the fitting on U - and Y -band images, because their S/N is too low.

3.3. Spectroscopy

Figure 2 shows the high S/N rest-frame UV spectrum of J1432+3358 taken using Gemini GMOS-N. The spectrum covers the rest-frame wavelength from 1100-1700 Å, and shows the strong Ly α emission line and a few absorption features from the interstellar medium (ISM) (e.g., Si II, O I, Si IV, and C IV). In the spectrum, there is no prominent N V 1240 emission line detected at the level of equivalent width of 2 Å (1 σ level) corresponding to rest-frame equivalent width (EW $_0$) of 0.5 Å, which is much smaller than the EW $_0$ of 18 ± 10 Å measured in a sample of bright quasars (Forster et al. 2001). Similarly, the C IV 1548, 1551 doublet line shows an absorption rather than emission feature.

J1432+3358 is not detected at the X-ray energies (0.5-7.0 keV) with 30 ks *Chandra* observation (P.I. Murray Obs ID 13134) (also see, Murray et al. 2005). The flux limit of the X-ray data is about 4×10^{-16} erg cm $^{-2}$ s $^{-1}$. By assuming the X-ray spectrum as a common AGN power-law spectrum with photon index $\Gamma = 1.7$ (e.g., Kenter et al. 2005), the Galactic neutral hydrogen column density $N_H = 1 \times 10^{20}$ cm $^{-2}$ (e.g., Dickey & Lockman 1990), and the X-ray-to-optical power-law slope $\alpha_{ox} = -1.45$ (e.g., Just et al. 2007), we find that less than 10% of the optical radiation could be from the AGN. J1432+3358 is not detected at 20cm in radio wavelength (de Vries et al. 2002), with 1 σ sensitivity limit of 28μ Jy corresponding to a specific luminosity of 4.7×10^{30} erg s $^{-1}$ Hz $^{-1}$. This radio limit can not put a good constraint on the AGN activity in J1432+3358 by adopting the relation between optical and radio luminosity derived from the SDSS quasar sample (White et al. 2007). The rest-frame NIR excess does not show in the *Spitzer* bands, which suggests absence of hot dust and obscured AGN. The IRAC [3.6]-[4.5] and [5.8]-[8.0] colors

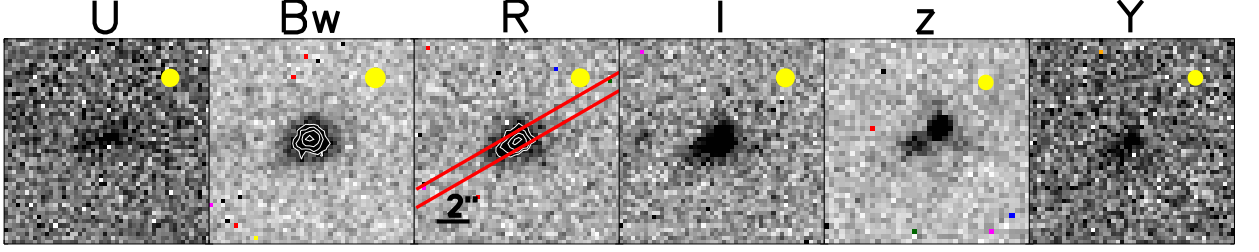


FIG. 1.— The U -, B_W -, R -, I -, z -, and Y -band images of J1432+3358. A contour plot is also shown in B_W - and R -band images. The yellow filled circles represent the size of point spread functions (PSF) in each image. The typical image qualities for U -, B_W -, R -, I -, z -, and Y -band images are $1''.0$, $1''.3$, $1''.2$, $1''.2$, $0''.5$ and $0''.6$, respectively. The slit position and orientation are also shown in R -band image.

TABLE 1
MAGNITUDE AND MORPHOLOGICAL PROPERTIES OF J1432+3358.

Filter	Magnitude ^a	r_e ^b	n ^c	b/a ^d	θ ^e	χ^2/ν ^f
U	24.35 ± 0.13	-	-	-	-	-
B_W	23.26 ± 0.02	0.73 ± 0.20	3.10 ± 0.77	0.49 ± 0.05	-73.17 ± 3.75	1.310
R	22.29 ± 0.03	0.89 ± 0.04	1.23 ± 0.27	0.45 ± 0.04	-63.81 ± 2.84	1.078
I	22.20 ± 0.03	0.82 ± 0.05	1.37 ± 0.37	0.38 ± 0.05	-55.04 ± 3.05	1.104
z	22.13 ± 0.03	-	-	-	-	-
$z(a)$ ^g	22.62 ± 0.04^i	0.26 ± 0.03	4	0.69 ± 0.08	14.04 ± 13.21	1.168
$z(b)$ ^h	23.71 ± 0.07^i	0.21 ± 0.03	1	0.67 ± 0.14	82.43 ± 19.12	1.168
Y	22.19 ± 0.09	-	-	-	-	-
H	21.54 ± 0.36	-	-	-	-	-
IRAC1	20.88 ± 0.06	-	-	-	-	-
IRAC2	20.66 ± 0.07	-	-	-	-	-
IRAC3	20.69 ± 0.37	-	-	-	-	-
IRAC4	20.42 ± 0.33	-	-	-	-	-

^aTotal AB magnitude from SExtractor.

^bEffective radius (") from the GALFIT fitting.

^cSérsic index from the GALFIT fitting.

^dThe ratio of minor axis (b) and major axis (a) from the GALFIT fitting.

^eThe position angle from the GALFIT fitting.

^fThe reduced chi-square from the GALFIT fitting.

^gThe GALFIT fitting results of the brighter components in z -band image.

^hThe GALFIT fitting results of the fainter components in z -band image.

ⁱThe magnitude is from the GALFIT fitting.

TABLE 2
LY α EMISSION AND STRONG INTERSTELLAR ABSORPTION LINES.

line	λ_{rest} ^a Å	λ_{obs} Å	EW Å	FWHM km s ⁻¹	redshift	Δv ^b km s ⁻¹
Ly α ^c	1215.08	4592.99 ± 0.59	34.97 ± 2.74	1431 ± 81	2.780 ± 0.000	392 ± 38
Ly $\alpha(a)$ ^d	1215.08	4597.41^g	27.46 ± 2.59	852 ± 56	2.784	680
Ly $\alpha(b)$ ^e	1215.08	4582.52^g	9.86 ± 1.38	1073 ± 151	2.771	-291
Ly $\alpha(c)$ ^f	1215.08	4601.05 ± 0.36	4.5 ± 1.5	200 ± 25	2.787	923 ± 25
Si II	1259.83	4752.42 ± 1.83	-1.89 ± 0.52	1004 ± 288	2.772 ± 0.001	-222 ± 115
O I	1302.69	4912.05 ± 4.33	-2.65 ± 0.89	2031 ± 643	2.771 ± 0.003	-346 ± 264
Si IV	1393.18	5274.68 ± 2.00	-2.11 ± 0.50	1041 ± 259	2.786 ± 0.001	872 ± 113
C IV	1548.91	5825.82 ± 2.41	-4.04 ± 0.83	1901 ± 384	2.761 ± 0.002	-1101 ± 123

^aAir wavelengths.

^bThe line velocity relative to the systemic redshift. The negative (positive) values correspond to blueshift (redshift).

^cThe whole Ly α emission.

^dThe primary peak of the Ly α emission corresponding to the 'a' component in Figure 2.

^eThe secondary peak of the Ly α emission corresponding to the 'b' component in Figure 2.

^fThe Ly α emission from the faint component corresponding to the 'c' component in Figure 2. The information of this component is derived from Extractor measurement and Gaussian fitting in the 2D spectra image.

^gTo deblend the two peaks of the Ly α emission line, the central wavelength values are set to the peak values of these two lines and fixed during the fitting.

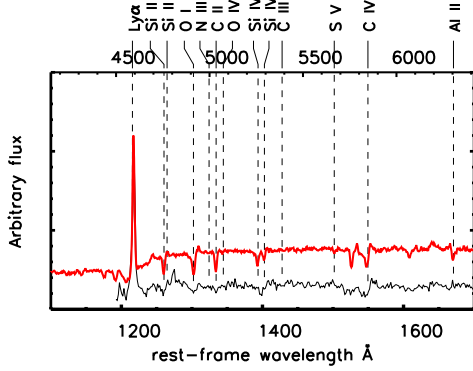


FIG. 2.— The rest-frame UV spectrum of J1432+3358 in the wavelength range 1100-1700 Å (the thin black solid curve). For comparison, the composite spectrum of a sample of $z \sim 3$ LBGs is also shown with a red thick solid curve (Shapley et al. 2003). The top x-axis represents the observed-frame wavelength. Both spectra are scaled by the peak value of the Ly α emission line, and the composite spectrum is shifted by +0.1 in flux density direction for clarity.

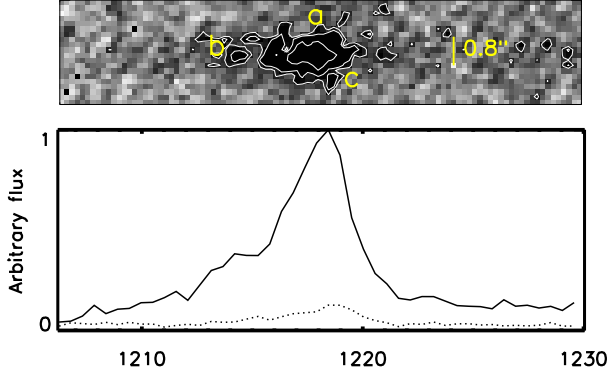


FIG. 3.— The 2D spectrum (top panel) and the 1D spectrum (bottom panel) of the Ly α emission line. There are 3 significant components resolved in 2D spectrum image. The components of 'a' and 'b' correspond to the redshifted stronger peak and the blueshifted weaker peak, respectively. The component of 'c' corresponds to the Ly α emission from the fainter component which was resolved in z -band image. The central wavelength difference between components 'a' and 'c' is about 3.6 Å.

are located out of the AGN selection area in MIR color-color space (e.g., Lacy et al. 2004; Stern et al. 2005). The rest-frame UV spectrum, the non-detection in X-ray and radio bands and MIR colors imply that there is no or only weak AGN ($< 10\%$) in J1432+3358, therefore, we suggest that the UV emission is dominated by the emission from massive stars rather than a central AGN.

The properties of the well detected ($S/N > 3$) lines in the rest-frame UV spectrum are listed in table 2. Because the observed wavelength of Ly α emission and ISM absorption lines are affected by galactic-scale outflows, the redshifts from these lines do not represent the systemic redshift (e.g., Adelberger et al. 2005). Typically, the systemic redshift can be derived from absorption lines that are clearly associated with photospheric features (e.g., S V 1502, C III 1176, O VI 1343, etc) (e.g.,

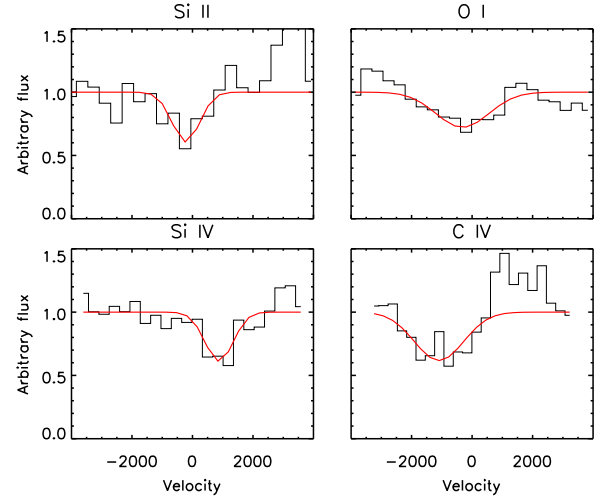


FIG. 4.— The spectra around the absorption lines (the back curves in histogram mode) and best-fit Gaussian models (the red curves). The flux is scaled by the continuum flux.

Dey et al. 1997; Shapley et al. 2003), but we can not identify these lines from the spectrum at current S/N level. Therefore, we follow Adelberger et al. (2005), in which they calibrate the redshifts of the Ly α and ISM absorption lines with the H α nebular line in a sample of $z \sim 2 - 3$ LBGs (see details in Adelberger et al. 2005). The scattering of this relation is less than 0.0015. Here the systemic redshift of J1432+3358 is estimated from the Ly α and absorption lines using the equations 1 and 2 in Steidel et al. (2010), which are 2.7745 and 2.7755, respectively. This result is also consistent with the systemic redshift calculated using the equation 3 in Adelberger et al. (2005). The systemic redshift of 2.775 ± 0.001 is adopted for further analysis in this paper.

The composite spectrum of LBGs at $z = 2 - 3$ is also shown in Figure 2 for comparison (Shapley et al. 2003). The continuum shape of the spectrum is similar to that of LBG composite spectrum, indicating that the dust extinction in J1432+3358 is similar to the dust extinction in the typical LBGs. This property is also supported by the SED fitting results (see details in section 3.4).

The prominent Ly α emission line is shown in Figures 3 and 2 with EW_0 of 35 Å. In Figures 3, the Ly α emission shows two peaks separated by 970 km s^{-1} and the full width at half maximum (FWHM) of the Ly α emission line is $\sim 1500 \text{ km s}^{-1}$, which is much larger than the $FWHM(\text{Ly}\alpha) = 450 \pm 150 \text{ km s}^{-1}$ typically found in $z \sim 3$ LBGs (Shapley et al. 2003). The secondary peak is real rather than noise, because the double-hump profile is exhibited in the individual spectra of the eight individual 30-min exposures. Two Gaussian profiles are used to deblend the Ly α emission lines. The FWHMs of the two Ly α components are $\sim 1000 \text{ km s}^{-1}$. Like most of the LBGs with multiply-peaked Ly α emission (Kulas et al. 2012), J1432+3358 shows stronger redshifted Ly α emission than blueshifted. The separation of the two Ly α peaks is $\sim 1000 \text{ km s}^{-1}$, which is comparable to the separation in other multiple-peaked LBGs (Kulas et al. 2012). Such a Ly α line profile is observed in the expansion shell model (Verhamme et al. 2006), which predicts that a primary Ly α peak is redshifted by approximately two times the expansion velocity and another blueshifted

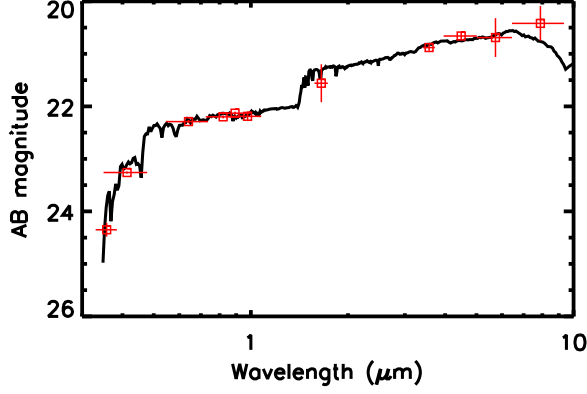


FIG. 5.— The best-fit stellar synthesis model (solid curve) and photometric data points from U -band to IRAC4-band (red squares).

$\text{Ly}\alpha$ emission is located around the expansion velocity.

In the 2-dimensional (2D) spectral image of the $\text{Ly}\alpha$ emission (Figure 3), there are three significant components of $\text{Ly}\alpha$ emission detected. The ‘a’ and ‘b’ components which are resolved in the wavelength direction correspond to the double-peak feature in the 1-dimensional (1D) spectrum. The ‘c’ component resolved in the slit (spatial) direction is the $\text{Ly}\alpha$ emission from the fainter component detected in the z -band image. To determine the wavelength of ‘c’ component, SExtractor and GALFIT are used to obtain the centroid and GAUSSIAN fitting central positions of ‘a’ and ‘c’ components. The offsets of the central wavelength between ‘a’ and ‘c’ components are 3.90 \AA and 3.25 \AA from the measurements with above two methods, respectively. We adopt the 3.64 ± 0.36 as the offset of the central wavelength between ‘a’ and ‘c’ components, which corresponds to a velocity difference of $237 \pm 23 \text{ km s}^{-1}$. The $\text{Ly}\alpha$ flux ratio between the components ‘a’ and ‘c’ is about 7:1 from the SExtractor measurement, which is higher than the continuum flux ratio between these two components. The velocity offset and the difference in flux ratio of $\text{Ly}\alpha$ and continuum in components of ‘a’ and ‘c’ also support that J1432+3358 is not a lensed system.

The spectrum also shows weak absorption lines originated from the interstellar median (ISM), which are Si II, O I, Si IV, and C IV lines (Figure 4). The EW_0 of these absorption features are a few \AA , comparable to those in typical LBGs. However, the FWHMs of these lines are 1000 km s^{-1} or even larger (Table 2), about two times larger than those in typical LBGs. The absorption lines show blueshifts with velocities of $200\text{--}1000 \text{ km s}^{-1}$, which can be interpreted by a galactic scale outflow model (Heckman et al. 2000; Steidel et al. 2010). The average outflows velocity estimated from Si II, O I and C IV absorption lines is $-556 \pm 103 \text{ km s}^{-1}$. We do not use the Si IV 1392 absorption line for the analysis, because the measurements of this line is contaminated by the S IV 1402 Steidel et al. (2010) find that average outflow velocity of LBGs derived from the ISM absorption lines is $164 \pm 16 \text{ km s}^{-1}$ with a wide range distribution from 0 to 500 km s^{-1} , and we find the outflow velocities in J1432+3358 are larger than the outflow velocities in most (> 98%) of LBGs. .

3.4. Physical Properties

An IDL-based code FAST (Fitting and Assessment of Synthetic Templates) (Kriek et al. 2009) is used to fit the broad band (U , B_W , R , I , Y , H , IRAC1, IRAC2, IRAC3, and IRAC4) photometry with stellar population synthesis models (Bruzual & Charlot 2003, BC03) and to derive the physical properties of J1432+3358. First, we use an exponential star formation rate ($\text{SFR} \propto \exp(-t_{\text{sf}}/\tau)$) with a Salpeter initial mass function (IMF) (Salpeter 1955) and solar metallicity. We adopt the dust extinction law proposed by Calzetti et al. (2000) and the intergalactic medium (IGM) absorption model in Madau (1995). From the SED fitting, we place constraints on the exponential star formation time scale, $\log(\tau(\text{yr})) = 10.00^{+1.00}_{-1.66}$. The large τ value indicates that the SFR declines slowly, suggesting that J1432+3358 has continuous constant star formation history. Therefore, we adopt a constant star formation history model for further analysis. In Figure 5, we show the best-fit spectral energy distribution overlaid on the optical (U , B_W , R , and I , Y), NIR (H), and MIR (IRAC1 ($3.6\mu\text{m}$), 2 ($4.5\mu\text{m}$), 3 ($5.8\mu\text{m}$), 4 ($8.0\mu\text{m}$)) photometry. From the fitting, we find that the galaxy age, $\log(t_{\text{sf}}(\text{yr})) = 8.8^{+0.2}_{-0.2}$, the SFR is $280^{+70}_{-60} \text{ M}_{\odot} \text{ yr}^{-1}$, the dust extinction is $E(B - V) = 0.12 \pm 0.02$, and the stellar mass is $(1.3 \pm 0.3) \times 10^{11} \text{ M}_{\odot}$. The SFR derived from the dust-corrected UV luminosity is $310 \text{ M}_{\odot} \text{ yr}^{-1}$ (Kennicutt 1998a), which is consistent with that derived from the SED fitting. The SFR in J1432+3358 thus is one order of magnitude higher than that in typical $z \sim 3$ LBGs (Shapley et al. 2001). The SED fitting suggests that the star formation age (t_{sf}) is about two times longer than the median star formation time in typical $z \sim 3$ LBG sample (Shapley et al. 2001). This age is also longer than the typical time scale of the starburst in submillimeter galaxies (SMGs), which is about 200 Myr (e.g., Narayanan et al. 2010). The star formation history and high stellar mass (about ten times higher than the median stellar mass in typical $z \sim 3$ LBG sample (Shapley et al. 2001)) in J1432+3358 indicate that it is a massive system with a long-term intensive star formation process rather than a low massive system which harbors a star formation burst. However, the physical properties derived from SED fitting are not reliable due to the weak constraints on the star formation time scale (τ). The star formation ages t_{sf} have significant degeneracies with the τ values (see details in Shapley et al. 2001, 2005), which could affect our above conclusion. On the other hand, the stellar mass estimation is much more reliable, because the rest-frame NIR M/L is reasonably constraint by the SED fitting and nearly independent on the τ values.

The gas mass can be estimated using the global Kennicutt-Schmidt law (Kennicutt 1998b):

$$\Sigma_{\text{gas}} = 361 \times \left(\frac{\Sigma_{\text{SFR}}}{1 \text{ M}_{\odot} \text{ yr}^{-1} \text{ kpc}^{-2}} \right)^{0.71} \text{ M}_{\odot} \text{ kpc}^{-2}, \quad (2)$$

where $\Sigma_{\text{SFR}} = \text{SFR}/r_e^2$ and the gas mass, M_{gas} , can be derived from $\Sigma_{\text{gas}} \times r_e^2$, which is $3.7 \times 10^{10} \text{ M}_{\odot}$. The fraction of gas in J1432+3358, $M_{\text{gas}}/(M_{\text{gas}} + M_{\text{stellar}})$, is 0.2. The low gas fraction is consistent with the gas fraction in the UV-selected galaxies at the most massive

end (Erb et al. 2006a) and comparable to that in submillimeter galaxies (Tacconi et al. 2008).

4. DISCUSSION

J1432+3358 shows unique properties compared to normal LBGs characterized by: (1) a high SFR (about $300 M_{\odot} \text{ yr}^{-1}$), (2) a 3:1 merger-like morphology with a $1.0''$ separation of the two components, (3) a high stellar mass ($1.3 \times 10^{11} M_{\odot}$), and (4) a long continuous star formation history (630 Myr), which is twice longer than median star formation history of LBGs.

One of the key questions is regarding the nature of UV ultra-luminous LBGs. By integrating the UV luminosity function (e.g., Reddy & Steidel 2009), we find that the space number density of the UV ultra-luminous LBGs with $L > 7L^*$ is a few 10^{-7} Mpc^{-3} in the redshift range from 2.7 to 3.3, which corresponds to a spatial number density of $\sim 0.3 \text{ deg}^{-2}$. This is consistent with the result that there is only one UV ultra-luminous LBG found in the 9 deg^2 NDWFS Boötes field within uncertainties. The space number density of UV ultra-luminous LBGs is about 2-3 orders of magnitude smaller than that of typical star-forming galaxies (e.g., LBGs, BzK galaxies) at $z \sim 2 - 3$, which is about $10^{-4} - 10^{-5} \text{ Mpc}^{-3}$ (e.g., Reddy et al. 2005). On the other hand, the space density of galaxy with its stellar mass greater than $10^{11} M_{\odot}$ is about 10^{-4} Mpc^{-3} based on the stellar mass function (e.g., Drory et al. 2005). The low space density of UV ultra-luminous LBGs can be interpreted by the following two different scenarios: the first one is that UV ultra-luminous LBGs can only be found in a short evolutionary phase for the most intensive star-forming galaxies. Though the SED-fitting result shows that the star formation time (t_{sf}) in J1432+3358 is 630 Myr, this galaxy may only be selected by UV-selection method during a short time period, i.e., most of the time the galaxy is highly obscured by dust. The other interpretation is that most of the galaxies that form stars at high intensity are dusty and highly obscured, e.g., SMGs (Chapman et al. 2005) or DOGs (dust-obscured galaxies) (Dey et al. 2008; Fiore et al. 2008), and only small fraction of galaxies that show high SFR is unobscured by dust.

Another crucial question is whether the extremely high SFR in J1432+3358 is triggered by galaxy major mergers or fueled by rapid accretion of cold gas from the intergalactic medium (IGM). Hopkins et al. (2008) investigate the role of mergers in the evolution of starburst and quasars and suggest an evolution track from a ‘typical’ galaxy to a gas-rich major merger (see a schematic outline in Figure 1 in Hopkins et al. 2008). In this scenario, at the early stage of merger, i.e. their phase (c), the two interacting galaxies are within one halo but still well separated and can be identified as a merger pair (e.g., Lotz et al. 2004). In this stage, the SFR starts to increase to about $100 M_{\odot} \text{ yr}^{-1}$ due to the tidal torques, but the enhanced effect of the SFR is relatively weak compared to the latter coalescence phase. The timescale of this phase is about several million years. The AGN

activity in this phase is relatively low. These features are consistent with the properties of J1432+3358.

A tight correlation between the stellar mass (M_{stellar}) and SFR (main sequence) in normal star forming galaxies has been found in both local and high-redshift universe (e.g., Daddi et al. 2007). The mean value of the specific SFR ($\text{sSFR} = \text{SFR}/M_{\text{stellar}}$) is about $1.8 \times 10^{-9} \text{ yr}^{-1}$ in star-forming galaxies at $z \sim 2$ at the high stellar mass end ($10^{11.0} M_{\odot} < M_{\text{stellar}} < 10^{11.5} M_{\odot}$). The galaxies with sSFR greater than $\sim 5.6 \times 10^{-9} \text{ yr}^{-1}$ are considered to be off the main sequence and suggested to be merger-driven starburst galaxies (e.g., Rodighiero et al. 2011). The sSFR of J1432+3358 is $1.9 \times 10^{-9} \text{ yr}^{-1}$, which would locate our galaxy right on the galaxy main sequence at $z \sim 2$. This result implies that the SFR in J1432+3358 is not enhanced by the merger process, which is also consistent that this system is in the early phase of the merger process. However, above conclusion is based on the SED fitting results which are subject to large systematic uncertainty as discussed in Section 3.3. Therefore, further high resolution space-based imaging and ground-based IFU observations will be requested to provide more firm evidence to distinguish whether J1432+3358 is a major merger or a clumpy disk galaxy.

The outflow properties of J1432+3358 can be studied and compared to the typical LBGs. Steidel et al. (2010) does not find a correlation between the SFR and the velocity of the wind in the UV-selected galaxies at $z \sim 2$, which is found in other high-redshift galaxies (Weiner et al. 2009). One interpretation is that the SFR dynamic range in Steidel et al. (2010) sample is too small to reveal the relation. With the SFR an order of magnitude higher than typical $z \sim 2$ UV-selected galaxies, J1432+3358 will provides enough dynamic range to check whether there exists correlation between the SFR and outflow velocity. Comparing J1432+3358 to the typical $z \sim 2$ UV-selected galaxies (Steidel et al. 2010), we do find that the outflow velocity increases with SFR, and roughly follows the relation found in Weiner et al. (2009), $v_{\text{out}} \propto \text{SFR}^{0.3}$.

We would like to thank the anonymous referee for providing constructive comments and help in improving the manuscript. This work made use of images and/or data products provided by the NOAO Deep Wide-Field Survey ((Jannuzi and Dey 1999), which is supported by the National Optical Astronomy Observatory (NOAO)). NOAO is operated by AURA, Inc., under a cooperative agreement with the National Science Foundation. We thank the LBTO, NOAO, and Gemini staff for their great support in preparing the observing and carrying out the observing. FB thanks M. Kriek for providing her IDL SED-fitting package and C. Peng for discussion on GALFIT. YTL is grateful to the HyperSuprimeCam software development team for the aid of reduction of the SuprimeCam data. FB, XF, LJ and IM acknowledge support from a Packard Fellowship for Science and Engineering and NSF grant AST 08-06861.

Facilities: LBT, MMT, Gemini-N, KPNO 4m Mayall, Spitzer, Subaru

REFERENCES

- Adelberger, K. L., Shapley, A. E., Steidel, C. C., Pettini, M., Erb, D. K., & Reddy, N. A. 2005, *ApJ*, 629, 636
- Adelberger, K. L., Steidel, C. C., Giavalisco, M., Dickinson, M., Pettini, M., & Kellogg, M. 1998, *ApJ*, 505, 18

- Allam, S. S., Tucker, D. L., Lin, H., Diehl, H. T., Annis, J., Buckley-Geer, E. J., & Frieman, J. A. 2007, *ApJ*, 662, L51
- Ashby, M. L. N., et al. 2009, *ApJ*, 701, 428
- Bentz, M. C., Pogge, R. W., & Osmer, P. S. 2008, *AJ*, 136, 498
- Bertin, E., & Arnouts, S. 1996, *A&AS*, 117, 393
- Bouwens, R. J., Illingworth, G. D., Franx, M., & Ford, H. 2008, *ApJ*, 686, 230
- Bouwens, R. J., et al. 2011, *Nature*, 469, 504
- Bruzual, G., & Charlot, S. 2003, *MNRAS*, 344, 1000
- Calzetti, D., Armus, L., Bohlin, R. C., Kinney, A. L., Koornneef, J., & Storchi-Bergmann, T. 2000, *ApJ*, 533, 682
- Chapman, S. C., Blain, A. W., Smail, I., & Ivison, R. J. 2005, *ApJ*, 622, 772
- Cooke, J., Barton, E. J., Bullock, J. S., Stewart, K. R., & Wolfe, A. M. 2008, *ApJ*, 681, L57
- Cowie, L. L., Songaila, A., Hu, E. M., & Cohen, J. G. 1996, *AJ*, 112, 839
- Daddi, E., et al. 2007, *ApJ*, 670, 156
- de Vries, W. H., Morganti, R., Röttgering, H. J. A., Vermeulen, R., van Breugel, W., Rengelink, R., & Jarvis, M. J. 2002, *AJ*, 123, 1784
- Dey, A., van Breugel, W., Vacca, W. D., & Antonucci, R. 1997, *ApJ*, 490, 698
- Dey, A., et al. 2008, *ApJ*, 677, 943
- Dickey, J. M., & Lockman, F. J. 1990, *ARA&A*, 28, 215
- Diehl, H. T., et al. 2009, *ApJ*, 707, 686
- Drory, N., Salvato, M., Gabasch, A., Bender, R., Hopp, U., Feulner, G., & Pannella, M. 2005, *ApJ*, 619, L131
- Erb, D. K., Shapley, A. E., Pettini, M., Steidel, C. C., Reddy, N. A., & Adelberger, K. L. 2006a, *ApJ*, 644, 813
- Erb, D. K., Steidel, C. C., Shapley, A. E., Pettini, M., Reddy, N. A., & Adelberger, K. L. 2006b, *ApJ*, 647, 128
- Ferguson, H. C., et al. 2004, *ApJ*, 600, L107
- Fiore, F., et al. 2008, *ApJ*, 672, 94
- Forster, K., Green, P. J., Aldcroft, T. L., Vestergaard, M., Foltz, C. B., & Hewett, P. C. 2001, *ApJS*, 134, 35
- Giallongo, E., et al. 2008, *A&A*, 482, 349
- Giavalisco, M. 1998, in *The Hubble Deep Field*, ed. M. Livio, S. M. Fall, & P. Madau, 121–+
- Giavalisco, M., Steidel, C. C., Adelberger, K. L., Dickinson, M. E., Pettini, M., & Kellogg, M. 1998, *ApJ*, 503, 543
- Heckman, T. M., Lehnert, M. D., Strickland, D. K., & Armus, L. 2000, *ApJS*, 129, 493
- Hill, J. M., Green, R. F., Ashby, D. S., Brynnel, J. G., Cushing, N. J., Little, J., Slagle, J. H., & Wagner, R. M. 2010, in *Society of Photo-Optical Instrumentation Engineers (SPIE) Conference Series*, Vol. 7733, Society of Photo-Optical Instrumentation Engineers (SPIE) Conference Series
- Hopkins, P. F., Hernquist, L., Cox, T. J., & Kereš, D. 2008, *ApJS*, 175, 356
- Jain, B., & Lima, M. 2011, *MNRAS*, 411, 2113
- Jannuzi, B. T., & Dey, A. 1999, in *Astronomical Society of the Pacific Conference Series*, Vol. 191, Photometric Redshifts and the Detection of High Redshift Galaxies, ed. R. Weymann, L. Storrie-Lombardi, M. Sawicki, & R. Brunner, 111–+
- Just, D. W., Brandt, W. N., Shemmer, O., Steffen, A. T., Schneider, D. P., Chartas, G., & Garmire, G. P. 2007, *ApJ*, 665, 1004
- Kennicutt, Jr., R. C. 1998a, *ARA&A*, 36, 189
- . 1998b, *ApJ*, 498, 541
- Kenter, A., et al. 2005, *ApJS*, 161, 9
- Kriek, M., van Dokkum, P. G., Labbé, I., Franx, M., Illingworth, G. D., Marchesini, D., & Quadri, R. F. 2009, *ApJ*, 700, 221
- Kulas, K. R., Shapley, A. E., Kollmeier, J. A., Zheng, Z., Steidel, C. C., & Hainline, K. N. 2012, *ApJ*, 745, 33
- Lacy, M., et al. 2004, *ApJS*, 154, 166
- Lee, K.-S., Giavalisco, M., Conroy, C., Wechsler, R. H., Ferguson, H. C., Somerville, R. S., Dickinson, M. E., & Urry, C. M. 2009, *ApJ*, 695, 368
- Lee, K.-S., Giavalisco, M., Gnedin, O. Y., Somerville, R. S., Ferguson, H. C., Dickinson, M., & Ouchi, M. 2006, *ApJ*, 642, 63
- Lilly, S. J., Le Fevre, O., Hammer, F., & Crampton, D. 1996, *ApJ*, 460, L1+
- Lin, H., et al. 2009, *ApJ*, 699, 1242
- Lotz, J. M., Primack, J., & Madau, P. 2004, *AJ*, 128, 163
- Madau, P. 1995, *ApJ*, 441, 18
- Madau, P., Ferguson, H. C., Dickinson, M. E., Giavalisco, M., Steidel, C. C., & Fruchter, A. 1996, *MNRAS*, 283, 1388
- Mehlert, D., et al. 2001, *A&A*, 379, 96
- Murray, S. S., et al. 2005, *ApJS*, 161, 1
- Narayanan, D., Hayward, C. C., Cox, T. J., Hernquist, L., Jonsson, P., Younger, J. D., & Groves, B. 2010, *MNRAS*, 401, 1613
- Peng, C. Y., Ho, L. C., Impey, C. D., & Rix, H.-W. 2002, *AJ*, 124, 266
- Reddy, N. A., Erb, D. K., Steidel, C. C., Shapley, A. E., Adelberger, K. L., & Pettini, M. 2005, *ApJ*, 633, 748
- Reddy, N. A., & Steidel, C. C. 2009, *ApJ*, 692, 778
- Rodighiero, G., et al. 2011, *ApJ*, 739, L40
- Salpeter, E. E. 1955, *ApJ*, 121, 161
- Sand, D. J., Treu, T., Ellis, R. S., & Smith, G. P. 2005, *ApJ*, 627, 32
- Sérsic, J. L. 1963, *Boletín de la Asociación Argentina de Astronomía La Plata Argentina*, 6, 41
- Shapley, A. E., Steidel, C. C., Adelberger, K. L., Dickinson, M., Giavalisco, M., & Pettini, M. 2001, *ApJ*, 562, 95
- Shapley, A. E., Steidel, C. C., Erb, D. K., Reddy, N. A., Adelberger, K. L., Pettini, M., Barmby, P., & Huang, J. 2005, *ApJ*, 626, 698
- Shapley, A. E., Steidel, C. C., Pettini, M., & Adelberger, K. L. 2003, *ApJ*, 588, 65
- Smail, I., et al. 2007, *ApJ*, 654, L33
- Spergel, D. N., et al. 2007, *ApJS*, 170, 377
- Steidel, C. C., Adelberger, K. L., Shapley, A. E., Pettini, M., Dickinson, M., & Giavalisco, M. 2003, *ApJ*, 592, 728
- Steidel, C. C., Bogosavljević, M., Shapley, A. E., Kollmeier, J. A., Reddy, N. A., Erb, D. K., & Pettini, M. 2011, *ApJ*, 736, 160
- Steidel, C. C., Erb, D. K., Shapley, A. E., Pettini, M., Reddy, N., Bogosavljević, M., Rudie, G. C., & Rakic, O. 2010, *ApJ*, 717, 289
- Steidel, C. C., Giavalisco, M., Pettini, M., Dickinson, M., & Adelberger, K. L. 1996, *ApJ*, 462, L17+
- Steidel, C. C., Shapley, A. E., Pettini, M., Adelberger, K. L., Erb, D. K., Reddy, N. A., & Hunt, M. P. 2004, *ApJ*, 604, 534
- Stern, D., et al. 2005, *ApJ*, 631, 163
- Tacconi, L. J., et al. 2008, *ApJ*, 680, 246
- Turner, E. L., Ostriker, J. P., & Gott, III, J. R. 1984, *ApJ*, 284, 1
- van der Burg, R. F. J., Hildebrandt, H., & Erben, T. 2010, *A&A*, 523, A74
- Verhamme, A., Schaerer, D., & Maselli, A. 2006, *A&A*, 460, 397
- Weiner, B. J., et al. 2009, *ApJ*, 692, 187
- White, R. L., Helfand, D. J., Becker, R. H., Glikman, E., & de Vries, W. 2007, *ApJ*, 654, 99